# Theory of Concentration Dependence in Drag Reduction by Polymers and of the Maximum Drag Reduction Asymptote

Roberto Benzi,[1] Emily S. C. Ching,[2] Nizan Horesh,[2,3] and Itamar Procaccia[2,3]
[1]*Dipartimento di Fisica and INFM, Università "Tor Vergata," Via della Ricerca Scientifica 1, I-00133 Roma, Italy*
[2]*Department of Physics, The Chinese University of Hong Kong, Shatin, Hong Kong*
[3]*Department of Chemical Physics, The Weizmann Institute of Science, Rehovot, 76100 Israel*
(Received 1 May 2003; published 20 February 2004)

A simple model of the effect of polymer concentration on the amount of drag reduction in turbulence is presented, simulated, and analyzed. The qualitative phase diagram of drag coefficient versus Reynolds number (Re) is recaptured in this model, including the theoretically elusive onset of drag reduction and the maximum drag reduction (MDR) asymptote. The Re-dependent drag and the MDR are analytically explained, and the dependence of the amount of drag on material parameters is rationalized.

DOI: 10.1103/PhysRevLett.92.078302 PACS numbers: 83.60.Yz, 47.50.+d, 83.80.Rs

"Drag reduction" refers to the intriguing phenomenon when the addition of a few tens of parts per million (by weight) of long-chain polymers to turbulent fluids can bring about a reduction of the friction drag by up to 80% [1–3]. The phenomenon is well documented since Toms discovered it accidentally in 1949 while studying the degradation of polymers. The phenomenon is important, and had been used to reduce the drag in oil pipes and to increase the jet height in fire engines. The pioneering work of Virk [1,2] had systematized and organized a huge amount of experimental information, but the fundamtental mechanism for the phenomenon has remained under debate for a long time [3–5]. All the *experimental* and many of the *numerical* [6–9] investigations of drag reduction focused on channel and pipe geometries; recently, however, it had been discovered by *numerical simulations* [10] of model equations of viscoelastic flows [like the finitely extensible nonlinear elastic-Peterline (FENE-P) model] that drag reduction appears also in homogeneous and isotropic turbulence when seeded with polymers. This brought about a new focus to the search for the mechanism for drag reduction, since the analysis of model equations without wall effects should suffice to uncover a mechanism. Indeed, in a recent paper [11] the FENE-P equations were simplified further to a shell model of viscoelastic flow which was shown to exhibit drag reduction whose mechanism could be fully explored analytically. In this Letter we present additional crucial progress where we demonstrate and explain two of the most prominent (and least understood) characteristics of drag reduction, i.e., the onset [as a function of Reynolds number (Re)] and the maximum drag reduction (MDR) asymptote.

To set up the issues we reproduce in Fig. 1 a typical experimental figure from Ref. [2] which refers to the dependence of the friction (or drag) coefficient in pipe flows on Re. For a pipe of radius $R$ and length $L$, with $\Delta p$, $\rho$, and $U$ being, respectively, the pressure drop across $L$, the fluid density, and the mean velocity over a section, the drag coefficient $f$ reads

$$f = \frac{\Delta p}{\rho U^2}\,\frac{R}{L} \qquad \text{(pipe flow)}. \tag{1}$$

Drag reduction is tantamount to, say, an increase in the throughput $U$ for a fixed pressure drop $\Delta p$ when polymer is added to the working fluid. In Fig. 1 one sees that for low Re there is no drag reduction: the drag coefficient of pure water is unchanged by the addition of small concentration of polymers. Then there is a sharp onset of drag reduction at a value of Re that does not depend on the concentration. From this point on the amount of drag reduction depends both on the concentration of the polymer and on Re. It was shown by Virk, however, that the amount of drag

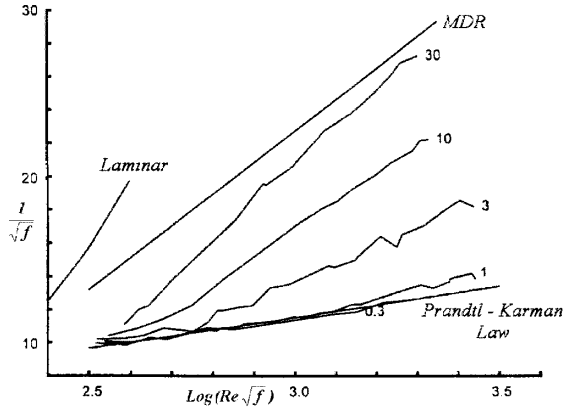


FIG. 1. Drag reduction in Prandtl-Karman coordinates [2]. As a function of Re the drag exhibits a (concentration independent) transition to drag reduction. The amount of drag reduction depends on the concentration until the asymptote denoted by MDR is reached. The Prandtl-Karman law is the Re-dependent drag of the neat fluid. The numbers indicate concentrations of the polymer additive in weight parts per million.

 0031-9007/04/92(7)/078302(4)$22.50  

reduction asymptotes to an apparently universal curve that cannot be exceeded by increasing the concentration further. This asymptote is referred to as the MDR, and was claimed to be insensitive to the nature of the polymer used in the experiments. In spite of the ample experimental evidence, both the onset and the existence of the MDR have not been theoretically understood. In this Letter we wish to close this gap.

Our strategy is to explore simulationally and analytically simplified models of viscoelastic flows which in spite of the simplification still represent the robust properties that we are after. As is well known, viscoelastic flows are represented well by hydrodynamic equations in which the effect of the polymer enters in the form of a "conformation tensor" $\boldsymbol{R}(\boldsymbol{r}, t)$ which stems from the ensemble average of the diadic product of the end-to-end distance of the polymer chains. Flexibility and finite extensibility of the polymer chains are reflected by the relaxation time $\tau$ and the Peterlin function $P(\boldsymbol{r}, t)$ which appear in the equation of motion for $\boldsymbol{R}$:

$$\frac{\partial R_{\alpha\beta}}{\partial t} + (\boldsymbol{u}\cdot\boldsymbol{\nabla})R_{\alpha\beta} = \frac{\partial u_\alpha}{\partial r_\gamma}R_{\gamma\beta} + R_{\alpha\gamma}\frac{\partial u_\beta}{\partial r_\gamma} - \frac{1}{\tau}[P(\boldsymbol{r}, t)R_{\alpha\beta} - \rho_0^2\delta_{\alpha\beta}], \quad (2)$$

$$P(\boldsymbol{r}, t) = (\rho_m^2 - \rho_0^2)/(\rho_m^2 - R_{\gamma\gamma}). \quad (3)$$

In these equations $\rho_m^2$ and $\rho_0^2$ refer to the maximal and the equilibrium values of the trace $R_{\gamma\gamma}$. Since in most applications $\rho_m \gg \rho_0$ the Peterlin function can also be written approximately as $P(\boldsymbol{r}, t) \approx 1/(1 - \alpha R_{\gamma\gamma})$ where $\alpha = \rho_m^{-2}$. In its turn the conformation tensor appears in the equations for fluid velocity $\boldsymbol{u}(\boldsymbol{r}, t)$ as an additional stress tensor:

$$\frac{\partial \boldsymbol{u}}{\partial t} + (\boldsymbol{u}\cdot\boldsymbol{\nabla})\boldsymbol{u} = -\boldsymbol{\nabla}p + \nu_s\nabla^2\boldsymbol{u} + \boldsymbol{\nabla}\cdot\boldsymbol{\mathcal{T}} + \boldsymbol{F}, \quad (4)$$

$$\boldsymbol{\mathcal{T}}(\boldsymbol{r}, t) = \frac{\nu_p}{\tau}\left[\frac{P(\boldsymbol{r}, t)}{\rho_0^2}\boldsymbol{R}(\boldsymbol{r}, t) - \mathbf{1}\right]. \quad (5)$$

Here $\nu_s$ is the viscosity of the neat fluid, $\boldsymbol{F}$ is the forcing, and $\nu_p$ is a viscosity parameter which is related to the concentration of the polymer, i.e., $\nu_p/\nu_s \sim c$ where $c$ is the volume fraction of the polymer. Note that the tensor field can be rescaled to get rid of the parameter $\alpha$ in the Peterlin function, $\tilde{\boldsymbol{R}}_{\alpha\beta} = \alpha R_{\alpha\beta}$ with the only consequence of rescaling the parameter $\rho_0$ accordingly. These equations were simulated on the computer in a channel or pipe geometry, reproducing faithfully the characteristics of drag reduction in experiments [6–8]. It should be pointed out, however, that even for present day computers simulating these equations is quite tasking. We therefore simplify the model further.

In developing a simple model we are led by the following ideas. First, it should be pointed out that all the nonlinear terms involving the tensor field $\boldsymbol{R}(\boldsymbol{r}, t)$ can be reproduced by writing an equation of motion for a vector field $\boldsymbol{B}(\boldsymbol{r}, t)$, and interpreting $R_{\alpha\beta}$ as the diadic product $B_\alpha B_\beta$. The relaxation terms with the Peterlin function are not automatically reproduced this way, and we need to add them by hand. Second, we should keep in mind that the above equations exhibit a generalized energy which is the sum of the fluid kinetic energy and the polymer free energy which is sensitive to the degree of polymer stretching by the turbulent flow. Led by these considerations we write the following shell model, which generalizes the one introduced in Ref. [11] and allows us to study also the effects of the polymer concentration:

$$\frac{du_n}{dt} = \frac{i}{3}\Phi_n(u, u) - \frac{i}{3}\frac{\nu_p}{\tau}P(B)\Phi_n(B, B) - \nu_s k_n^2 u_n + F_n,$$
$$\frac{dB_n}{dt} = \frac{i}{3}\Phi_n(u, B) - \frac{i}{3}\Phi_n(B, u) - \frac{1}{\tau}P(B)B_n - \nu_B k_n^2 B_n,$$
$$P(B) = \frac{1}{1 - \sum_n B_n^* B_n}. \quad (6)$$

In these equations $u_n$ and $B_n$ stand for the Fourier amplitudes $u(k_n)$ and $B(k_n)$ of the two respective vector fields, but as usual in the shell model we take $n = 0, 1, 2, \ldots$, and the wave vectors are limited to the set $k_n = 2^n$. The nonlinear interaction terms take the explicit form

$$\Phi_n(u, B) = k_n[(1-b)u_{n+2}B_{n+1}^* + (2+b)u_{n+1}^*B_{n+2}] + k_{n-1}[(2b+1)u_{n-1}^*B_{n+1} - (1-b)u_{n+1}B_{n-1}^*] + k_{n-2}[(2+b)u_{n-1}B_{n-2} + (2b+1)u_{n-2}B_{n-1}], \quad (7)$$

with an obvious simplification for $\Phi_n(u, u)$ and $\Phi_n(B, B)$. Here $b$ is a parameter taken below to be $-0.2$. In accordance with the generalized energy of the FENE-P model, our shell model has also the total energy

$$E \equiv \frac{1}{2}\sum_n |u_n|^2 - \frac{1}{2}\frac{\nu_p}{\tau}\ln\left(1 - \sum_n |B_n|^2\right). \quad (8)$$

The second term in the generalized energy contributes to the dissipation a positive definite term of the form $(\nu_p/\tau^2)P^2(B)\sum_n |B_n|^2$. With $\nu_p = 0$ the first of Eqs. (6) reduces to the well-studied Sabra model of Newtonian turbulence [12]. We therefore refer to the model with $\nu_p \neq 0$ as the SabraP model (the Sabra model with polymers). As in the FENE-P case we consider $\nu_p/\nu_s$ to be $c$. All the simulations below are performed with a constant rate of energy input, choosing $F_n = \phi/u_n^*$ for $n = 0, 1$ and zero otherwise.

In [11] it was shown that this shell model exhibits drag reduction, and the mechanism for the phenomenon was elucidated. The basic phenomenon is exhibited well by the spectra of the $u_n$ and $B_n$ fields which are presented at one value of the parameters in Fig. 2. The spectra for the Sabra model (dashed line) and the SabraP model (line)

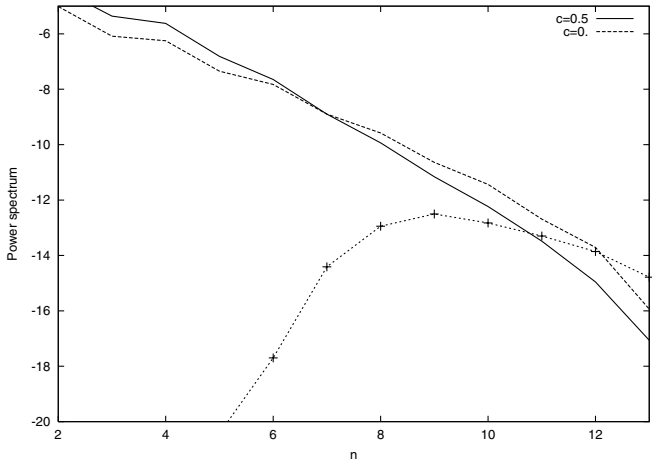


FIG. 2. Power spectra of the SabraP model (line) and the Sabra model (dashed line) for $\phi = 0.001$, $\nu_s = 10^{-6}$, and $\tau = 0.4$. The dashed line with symbols represents the power spectrum of the $B_n$ field.

are compared for the same amount of power input per unit time. The discussion [11] of the spectra revolves around the typical Lumley scale $k_c$ which is determined by the condition [4]

$$u(k_c)k_c \approx \tau^{-1}. \tag{9}$$

For $k_n \gg k_c$ the decay time $\tau$ becomes irrelevant for the dynamics of $B_n$. The nonlinear interaction between $u_n$ and $B_n$ at these scales results in both of them having the same spectral exponent which is also the same as that of the Sabra model. The amplitude of the $u_n$ spectrum is, however, smaller in the SabraP model compared to the Sabra case, since the $B_n$ field adds to the dissipation. On the other hand, for $k_n \ll k_c$ the $B_n$ field is exponentially suppressed by its decay due to $\tau$, and the spectral exponent of $u_n$ is again as in the Sabra model. Drag reduction comes about due to the interactions at length scales of the order of $k_c$ which force a strong tilt in the $u_n$ spectrum there, causing it to cross the Sabra spectrum, leading to an increase in the amplitude of the energy containing scale. This is why the kinetic energy is increasing for the same amount of power input, and hence drag reduction. Note that a very similar spectral crossover had been documented also in experiments [13] and in the FENE-P model in channel flow simulations [9].

The qualitative phenomena that we are about to explain in this Letter are demonstrated in the simulational results presented in Fig. 3. Here we show the drag coefficient $f$ as a function of Re for the Sabra and for the SabraP models for various values of the concentration. The drag coefficient is computed in analogy to Eq. (1) as

$$f \equiv \frac{\sum_n F_n u_n^*}{(\sum_n |u_n|^2)^{3/2} k_0} \qquad \text{(our model)}. \tag{10}$$

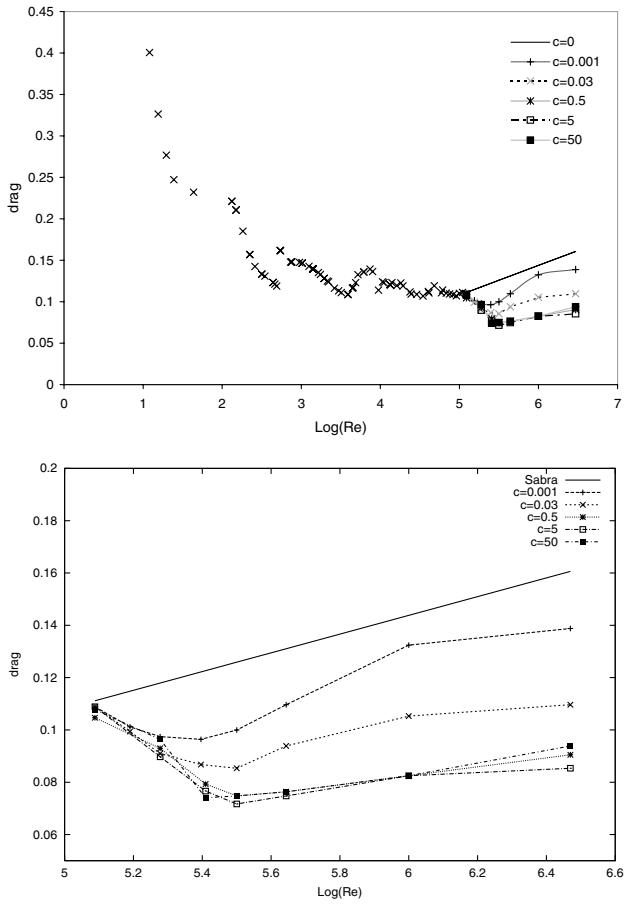


FIG. 3. Upper panel: Drag as a function of $\log_{10}(\mathrm{Re})$ including the laminar and the turbulent regimes. Both regimes agree with the Eqs. (11) and (12). Lower panel: Blowup of the turbulent regime. In both panels the upper straight line indicates the drag of the neat fluid, whereas the MDR is seen as the convergence of the drag data for large concentrations.

We observe all the phenomena discovered by Virk: (i) For the model of the neat fluid the drag has a laminar branch and a turbulent branch, with a sharp transition between them. (ii) For the model of the viscoelastic flow in the laminar region there is no drag reduction; the laminar branch is not changed by the addition of polymer with any concentration. (iii) Drag reduction has an onset that is independent of the concentration of the polymer. (iv) As the concentration increases, the amount of drag reduction increases, but (v) there exists an asymptote which is not exceeded when the concentration is increased. In other words, our simple model appears to reproduce extremely well the phenomena that were uncovered in so many experiments as summarized by Virk.

Next we explain all these observations. First we rationalize the Re dependence of the friction factor in the Sabra model of the neat fluid. For low Re the nonlinear terms $\Phi_n(u, u)$ are negligible compared to the viscous term. With forcing only on the largest scale $k_0$ we can evaluate

$$\nu_s k_0^2 u_0 \approx F_0 \to f \sim \frac{\nu_s k_0}{|u_0|} = \mathrm{Re}^{-1}, \qquad \text{for Re small.} \tag{11}$$

For large Re we have the exact result [12] that the third order correlation function $S_n^{(3)} \equiv \mathrm{Im}\langle u_{n-1} u_n u_{n+1}^* \rangle = C\bar{\epsilon}/k_n$ with $\bar{\epsilon}$ being the mean energy flux and $C$ a known constant (the analog of the 4/5th law for Navier-Stokes turbulence). We therefore expect the friction factor to tend to a constant value for large Re (up to terms $\sim \ln \mathrm{Re}$),

$$f \sim \mathrm{Re}^0, \qquad \text{Re large.} \tag{12}$$

Equations (11) and (12) (which are the analogs of the Prandtl-Karman law for pipe flows) are well borne out by the data in Fig. 3 for the model of the neat fluid. The laminar branch, which is exponential in these coordinates [$f \sim \exp\{-\log(\mathrm{Re})\}$], is unaffected by changing the concentration $c$. The transition between the two branches is expected when turbulence sets in, i.e., for Re such that the dissipative terms just begin to be overwhelmed by the nonlinear interactions. Thus, point (i) is understood. Note that similar arguments will hold for the FENE-P equations in homogeneous flows. Points (ii) and (iii) are explained as follows: we said above that drag reduction comes about due to the interaction between the two dynamical fields at a scale of the order of $k_c$. Clearly, as long as $k_c$ exceeds the dissipative scale $k_d$ of the $u_n$ field, no interaction between the two fields can be of any significance. Since $k_d$ is of the order of $k_d \sim k_0 \mathrm{Re}^{3/4}$, we can expect a concentration independent onset of drag reduction when $k_c \approx k_d$. Using $u_n \sim u_0 (k_n/k_0)^{-1/3}$, $k_c$ can be estimated as $k_c \sim k_0 (\tau u_0 k_0)^{-3/2}$, and we end up with a prediction for the onset of drag reduction when

$$\mathrm{Re} \approx (\tau u_0 k_0)^{-2}. \tag{13}$$

This prediction is well borne out by our simulations (because of the space constraint we do not display simulations at different values of $\tau$ and $k_0$). Again we point out that similar arguments can be presented for the FENE-P model as well.

Point (iv) is obvious—when the concentration increases, the mechanism discovered in [11] comes into play. What remains to be explained is the asymptotic MDR. This also follows directly from the analysis of the equations. Consider Eqs. (6) for two values of the parameter $\nu_p$, $\nu_p^{(1)} \ll \nu_p^{(2)}$, with $y^2 = \nu_p^{(1)}/\nu_p^{(2)}$. Rescaling $B_n$ according to $B_n = y\tilde{B}_n$, we see that the Peterlin function tends to unity when $y \to 0$,

$$P(\tilde{B}) = \frac{1}{1 - y^2 \sum_n |\tilde{B}_n|^2} \to 1, \qquad \text{when } y \to 0. \tag{14}$$

When $P(\tilde{B}) \approx 1$ the dynamical equation for $\tilde{B}_n$ is independent of $y$ due to its linearity, whereas the $u_n$ equation remains independent due to the rescaling:

$$\frac{i}{3} \frac{\nu_p^{(2)}}{\tau} P(B) \Phi_n(B, B) \to \frac{i}{3} \frac{\nu_p^{(1)}}{\tau} P(\tilde{B}) \Phi_n(\tilde{B}_n, \tilde{B}_n). \tag{15}$$

Thus, increasing the concentration brings the dynamical equations to an asymptotic concentration invariant form and therefore to an asymptotic MDR. For the last time we note that similar rescalings are also available in the FENE-P equations, making the points discussed here quite general for any sensible model of viscoelastic flow.

In summary, we have presented a simple model of drag reduction for which the observed characteristics can be explained on the basis of the equations of motion. It remains to go back to channel and pipe simulations of the FENE-P equations to demonstrate that the discussion presented above includes the main phenomena observed also there.

This work was supported in part by the European Commission under a TMR grant, the Minerva Foundation, Munich, Germany, and the Naftali and Anna Backenroth-Bronicki Fund for Research in Chaos and Complexity. E. S. C. C. acknowledges the Hong Kong Research Grants Council for support (CUHK 4046/02P).

[1] P. S. Virk, AIChE J. **21**, 625 (1975); Nature (London) **253**, 109 (1975).
[2] P. S. Virk, D. C. Sherman, and D. L. Wagger, AIChE J. **43**, 3257 (1997).
[3] K. R. Sreenivasan and C. M. White, J. Fluid Mech. **409**, 149 (2000).
[4] J. L. Lumley, Annu. Rev. Fluid Mech. **1**, 367 (1969).
[5] P.-G. de Gennes, *Introduction to Polymer Dynamics* (Cambridge University Press, Cambridge, 1990).
[6] J. M. J de Toonder, M. A. Hulsen, G. D. C. Kuiken, and F. T. M Nieuwstadt, J. Fluid Mech. **337**, 193 (1997).
[7] C. D. Dimitropoulos, R. Sureshdumar, and A. N. Beris, J. Non-Newtonian Fluid Mech. **79**, 433 (1998).
[8] E. de Angelis, C. M. Casciola, and R. Piva, Comput. Fluid Dyn. J. **9**, 1 (2000).
[9] E. De Angelis, C. M. Casciola, V. S. L'vov, R. Piva, and I. Procaccia, Phys. Rev. E **67**, 056312 (2003).
[10] E. de Angelis, C. Casciola, R. Benzi, and R. Piva (to be published).
[11] R. Benzi, E. De Angelis, R. Govindarajan, and I. Procaccia, Phys. Rev. E **68**, 016308 (2003).
[12] V. S. L'vov, E. Podivilov, A. Pomyalov, I. Procaccia, and D. Vandembroucq, Phys. Rev. E **58**, 1811 (1998).
[13] P. Tong, W. I. Goldburg, and J.S. Huang, Phys. Rev. A **45**, 7231 (1992).